An Improved Core-Corona Model for Λ and $\overline{\Lambda}$ Polarization in Relativistic Heavy-Ion Collisions

Alejandro Ayala [1,2,3], Isabel Dominguez [4], Ivonne Maldonado [5,*] and Maria Elena Tejeda-Yeomans [6]

1 Instituto de Ciencias Nucleares, Universidad Nacional Autónoma de México, Apartado Postal 70-543, Mexico City 04510, Mexico
2 Centre for Theoretical and Mathematical Physics, Department of Physics, University of Cape Town, Rondebosch 7700, South Africa
3 Departamento de Física, Universidade Federal de Santa Maria, Santa Maria 97105-900, RS, Brazil
4 Facultad de Ciencias Físico-Matemáticas, Universidad Autónoma de Sinaloa, Avenida de las Américas y Boulevard Universitarios, Ciudad Universitaria, Culiacán 80000, Mexico
5 Joint Institute for Nuclear Research, Dubna 141980, Russia
6 Facultad de Ciencias—CUICBAS, Universidad de Colima, Bernal Díaz del Castillo No. 340, Col. Villas San Sebastián, Colima 28045, Mexico
* Correspondence: maldonado@jinr.ru

Abstract: Due to its sensitivity to the dynamics of strongly interacting matter subject to extreme conditions, hyperon global polarization has become an important observable to study the system created in relativistic heavy-ion collisions. Recently, the STAR and HADES collaborations have measured the global polarization of both Λ and $\overline{\Lambda}$ produced in semi-central collisions in a wide range of collision energies. The polarization excitation functions show an increasing trend as the collision energy decreases, with the increase being more pronounced for the $\overline{\Lambda}$. In this work, we make a summary of a core-corona model that we have developed to quantify the global polarization contributions from Λ and $\overline{\Lambda}$ created in different regions of the fireball. The core-corona model assumes that Λs and $\overline{\Lambda}$s are produced in both regions, the high-density core and the lower density corona, with different relative abundances which modulate the polarization excitation function. We have shown that the model works well for the description of experimental results. The global polarization excitation functions computed with the model show a peak at different collision energies in the region $\sqrt{s_{NN}} \leq 10$ GeV. Finally, we discuss and report on the model global polarization predictions for BES-II, NICA and CBM at FAIR and HADES energies.

Keywords: hyperon; global polarization; core-corona; heavy-ion collisions; spin

1. Introduction

The global polarization of hyperons has recently gained great interest given its sensitivity to study aspects of the strongly interacting matter created in heavy-ion collisions such as vorticity, viscosity and flow. It can also provide information about the onset of criticality in the phase diagram [1–13]. In a non-central collision, the system acquires a large angular momentum along the direction of the transverse plane. This angular momentum can be quantified in terms of the thermal vorticity, which could be partially transferred to the spin degrees of freedom of particles created in the collision. The self-analysing properties of Λ and $\overline{\Lambda}$ particles through their charged decay are useful to measure this global polarization. Recently, the STAR-BES and HADES collaborations measured the Λ and $\overline{\Lambda}$ global polarizations for different collision energies [14–17]. These measurements show several interesting features: the polarizations increase as the energy of the collision decreases, and the increase is more pronounced for the $\overline{\Lambda}$. The polarizations show what seem to be maximum values close to the Λ production threshold energy in pp collisions which then decrease for lower energies. The system created at BES-I energies is dominated

by a QGP phase, so the global polarization at these energies is understood as a mechanism where this highly vortical fluid modifies the spin properties of hadrons produced at later stages. In systems created at lower energies, the QGP phase coexists with a baryon rich environment, so the polarization mechanism could be driven mainly by baryon dominated processes. Understanding the subtleties of the different mechanisms, by which global polarization is transferred to hyperons at BES-II, HADES, CBM at FAIR and NICA energies, can provide another important tool to pinpoint the critical phenomena expected to emerge at these energies. In order to contribute to this effort, we have developed a core-corona model [18–22]. In this contribution, we summarize the main components of this model, and we compare its predictions for Λ and $\overline{\Lambda}$ global polarization with experimental data at BES-II and HADES energies. We show that the model works well in the description of experimental results. We predict the presence of a maximum for each of the global polarizations at different collision energies in the region $\sqrt{s_{NN}} \leq 10$ GeV. Finally, we comment on current progress for the core-corona model improvement and the feasibility of global polarization measurements at NICA, HADES and CBM at FAIR energies.

2. A Core-Corona Model for $\Lambda/\overline{\Lambda}$ Polarization

In the core-corona model, the system is assumed to be formed with distinct density regions, as sketched in Figure 1. The overlap of the two colliding ions consists of a core in the central part and a corona in the periphery. We model the core as a region with a high enough density of participants to create a thermalized QGP fireball, while in the corona the interactions are more like those in pp collisions. Consequently, the particles that come from each region have different characteristics due to their different hadronisation mechanisms, by QGP or recombination processes, and interaction with the surrounding environment. We expect that observables, such as the polarization, will show a dependence not only in the collision energy and/or centrality, but also in the relative abundances of particles coming from the core and the corona, and its polarization mechanism associated with each region.

A+A
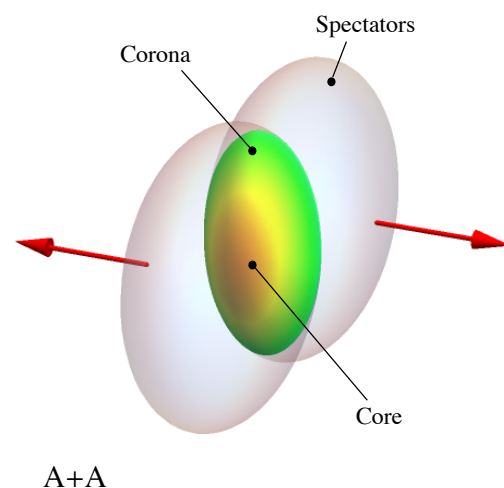
Figure 1. Sketch of a non-central heavy-ion collision. The non-homogeneity density of the fireball is illustrated by the color gradient. The core, in which Λs and $\overline{\Lambda}$s are produced by QGP processes, and the corona which is dominated by nucleon nucleon/N + N) reactions. The figure is taken from Ref. [18]).

In the core-corona scenario, the Λ average global polarization, $\mathcal{P}^{\Lambda}$, is defined as

$$\mathcal{P}^{\Lambda} = \frac{(N^{\uparrow}_{\Lambda\,\text{QGP}} + N^{\uparrow}_{\Lambda\,\text{REC}}) - (N^{\downarrow}_{\Lambda\,\text{QGP}} + N^{\downarrow}_{\Lambda\,\text{REC}})}{(N^{\uparrow}_{\Lambda\,\text{QGP}} + N^{\uparrow}_{\Lambda\,\text{REC}}) + (N^{\downarrow}_{\Lambda\,\text{QGP}} + N^{\downarrow}_{\Lambda\,\text{REC}})}, \tag{1}$$

and, similarly for the $\overline{\Lambda}$ average global polarization, $\mathcal{P}^{\overline{\Lambda}}$, is given by

$$\mathcal{P}^{\overline{\Lambda}} = \frac{(N^{\uparrow}_{\overline{\Lambda}\,\text{QGP}} + N^{\uparrow}_{\overline{\Lambda}\,\text{REC}}) - (N^{\downarrow}_{\overline{\Lambda}\,\text{QGP}} + N^{\downarrow}_{\overline{\Lambda}\,\text{REC}})}{(N^{\uparrow}_{\overline{\Lambda}\,\text{QGP}} + N^{\uparrow}_{\overline{\Lambda}\,\text{REC}}) + (N^{\downarrow}_{\overline{\Lambda}\,\text{QGP}} + N^{\downarrow}_{\overline{\Lambda}\,\text{REC}})}, \tag{2}$$

the ratio of the difference between the number of particles with their spin pointing along (up arrow) and opposite (down arrow) to a given direction, to their sum. In both Equations (1) and (2), we have used the total number of Λs ($\overline{\Lambda}$s), and $N_{\Lambda} = N_{\Lambda\,\text{QGP}} + N_{\Lambda\,\text{REC}}$ ($N_{\overline{\Lambda}} = N_{\overline{\Lambda}\,\text{QGP}} + N_{\overline{\Lambda}\,\text{REC}}$) is given as the sum of the number of Λs ($\overline{\Lambda}$s) coming from the core $N_{\Lambda\,\text{QGP}}$ ($N_{\overline{\Lambda}\,\text{QGP}}$) and the number of Λs ($\overline{\Lambda}$s) coming from the corona, $N_{\Lambda\,\text{REC}}$ ($N_{\overline{\Lambda}\,\text{REC}}$). Throughout this manuscript, the subscripts QGP and REC refer to the type of hadronisation mechanism involved in each region, by a coalescence-type of processes in the QGP, in the core and recombination of a di-quark(antiquark) with an s-quark(antiquark) as in pp collisions in the corona, respectively.

Next, we define the intrinsic polarization of Λs and $\overline{\Lambda}$s coming from the core as

$$z = \frac{N^{\uparrow}_{\Lambda\,\text{QGP}} - N^{\downarrow}_{\Lambda\,\text{QGP}}}{N_{\Lambda\,\text{QGP}}} \qquad \text{and} \qquad \bar{z} = \frac{N^{\uparrow}_{\overline{\Lambda}\,\text{QGP}} - N^{\downarrow}_{\overline{\Lambda}\,\text{QGP}}}{N_{\overline{\Lambda}\,\text{QGP}}}, \tag{3}$$

which helps to highlight the importance of the relative number of each kind of hyperon with spin aligned in opposite directions in each region, with respect to the total number of hyperons in that same region. Analogously, we identify the contribution to the global polarization from the corona as

$$\mathcal{P}^{\Lambda}_{\text{REC}} = \frac{N^{\uparrow}_{\Lambda\,\text{REC}} - N^{\downarrow}_{\Lambda\,\text{REC}}}{N_{\Lambda\,\text{REC}}} \qquad \text{and} \qquad \mathcal{P}^{\overline{\Lambda}}_{\text{REC}} = \frac{N^{\uparrow}_{\overline{\Lambda}\,\text{REC}} - N^{\downarrow}_{\overline{\Lambda}\,\text{REC}}}{N_{\overline{\Lambda}\,\text{REC}}}. \tag{4}$$

We can now rewrite the average global polarization $\mathcal{P}^{\Lambda}$ and $\mathcal{P}^{\overline{\Lambda}}$ from Equations (1) and (2) as

$$\mathcal{P}^{\Lambda} = \frac{\mathcal{P}^{\Lambda}_{\text{REC}} + z\frac{N_{\Lambda\,\text{QGP}}}{N_{\Lambda\,\text{REC}}}}{1 + \frac{N_{\Lambda\,\text{QGP}}}{N_{\Lambda\,\text{REC}}}}, \qquad \mathcal{P}^{\overline{\Lambda}} = \frac{\mathcal{P}^{\overline{\Lambda}}_{\text{REC}} + \bar{z}(\frac{w'}{w})\frac{N_{\Lambda\,\text{QGP}}}{N_{\Lambda\,\text{REC}}}}{1 + (\frac{w'}{w})\frac{N_{\Lambda\,\text{QGP}}}{N_{\Lambda\,\text{REC}}}}, \tag{5}$$

where the ratios $w' = N_{\overline{\Lambda}\,\text{QGP}}/N_{\Lambda\,\text{QGP}}$ and $w = N_{\overline{\Lambda}\,\text{REC}}/N_{\Lambda\,\text{REC}}$ control the antiparticle to particle relative abundances within the same region. Equation (5) shows that the Λ and $\overline{\Lambda}$ polarizations are governed by z, $\bar{z}$, $\mathcal{P}^{\Lambda}_{\text{REC}}$, $\mathcal{P}^{\overline{\Lambda}}_{\text{REC}}$, w, w', and the ratio $N_{\Lambda\,\text{QGP}}/N_{\Lambda\,\text{REC}}$. The dependence of these variables, with respect to collision energy and centrality, can be determined either from calculations or from experimental data. In the Appendices A–C, we provide a brief summary of the procedures to fix w, w', and the ratio $N_{\Lambda\,\text{QGP}}/N_{\Lambda\,\text{REC}}$, respectively.

3. Λ ($\overline{\Lambda}$) Intrinsic Polarization z ($\bar{z}$)

In order to calculate the intrinsic global Λ and $\overline{\Lambda}$ polarizations from the core, we assume that the s- and $\bar{s}$-quark polarizations, z and $\bar{z}$, respectively, translate into the Λ and $\overline{\Lambda}$ polarizations during the hadronisation process. This allows us to express the intrinsic polarization z (or $\bar{z}$) in terms of the relaxation time τ (or $\bar{\tau}$), that is, the time required by the corresponding quark to align its spin with the thermal vorticity ω, as a function of the QGP lifetime, $\Delta\tau_{QGP}$ [23],

$$\begin{aligned} z &= 1 - e^{-\Delta\tau_{QGP}/\tau}, \\ \bar{z} &= 1 - e^{-\Delta\tau_{QGP}/\bar{\tau}}. \end{aligned} \tag{6}$$

τ (or $\bar{\tau}$) is computed as the inverse of the total interaction rate $\tau \equiv 1/\Gamma$. The interaction rate is obtained from the imaginary part of the self-energy Σ of a quark with four-momentum $P = (p_0, \vec{p})$ as

$$\Gamma(p_0) = \tilde{f}(p_0) \text{Tr}[\gamma^0 \text{Im}\Sigma] \tag{7}$$

where $\tilde{f}(p_0)$ is the Fermi–Dirac distribution. The interaction between the spin and the thermal vorticity ω is modeled within the medium by means of a vertex coupling quarks and thermal gluons, as depicted in Figure 2.
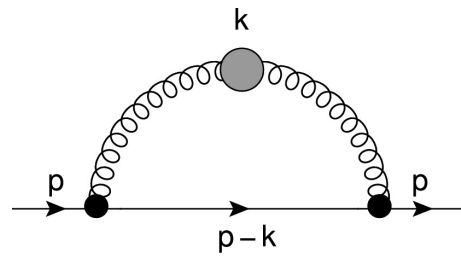
Figure 2. The interaction rate is obtained from the imaginary part of the self-energy, whose kinematics are defined by the one-loop self-energy quark diagram used to compute the interaction rate. The gluon line with a blob represents the effective gluon propagator at finite density and temperature. The blobs on the quark–gluon vertices represent the effective coupling between the quark spin and the thermal vorticity. The figure is taken from Ref. [22].

Equation (7) can be rewritten as [23]

$$\Gamma(p_0) = \frac{\alpha_s}{4\pi}\left(\frac{\omega}{T}\right)^2 \frac{C_F}{\sqrt{p_0^2 - m_q^2}} \int_0^\infty dk\, k \int_{\mathcal{R}} dk_0 [1 + f(k_0)]$$
$$\times \tilde{f}(p_0 + k_0 - \mu_q) \sum_{i=L,T} C_i(p0, k_0, k)\rho_i(k_0, k), \tag{8}$$

where the integral is performed over the kinematically available region, weighted with the statistical distributions, Bose-Einstein f for gluons and Fermi–Dirac $\tilde{f}$ for quarks. The temperature T is the μ_B-dependent freeze-out temperature. These quantities are explicitly given in Appendix B. The thermal vorticity ω is computed from the initial angular vorticity of events simulated with UrQMD [24,25]. C_i with $i = T, L$ are the result of the trace calculation after contraction of the transverse and longitudinal projection operators that come together with the gluon spectral functions ρ_i, the quark propagator and the vertices, after summing over the Matsubara frequencies.

The total interaction rate is obtained by integrating over the available phase space

$$\Gamma = V \int \frac{d^3 p}{(2\pi)^3} \Gamma(p_0), \tag{9}$$

where V is the volume of the core region.

The volume of the core is computed as $V = \pi R^2 \Delta\tau_{QGP}$, which depends on the collision energy as well as on the QGP life-time

$$\Delta\tau_{QGP} = A \ln \sqrt{s_{NN}} \tag{10}$$

with $A = 0.6803 \pm 0.05509, 1.116 \pm 0.09444$. This parametrization is obtained from the fit to the experimental distribution calculated with $\Delta\tau_{QGP} = \tau_f - \tau_0 = \tau_0[(\frac{T_0}{T_f})^3 - 1]$ where we assumed a Bjorken expansion in which the elapsed time between the initial formation τ_0 and the hadronisation τ_f times is related with the corresponding temperatures T_0 and T_f.

The initial temperature is extracted from experimental data from transverse momentum distributions of ϕ mesons, whereas the final temperature corresponds to the tempera-

ture along the chemical freeze-out curve, given in Appendix B. We choose $\tau_0 = 0.35, 0.60$ fm to fit the different centrality data.

The intrinsic polarization obtained for collisions at $b = 7.26$ fm is shown in Figure 3.
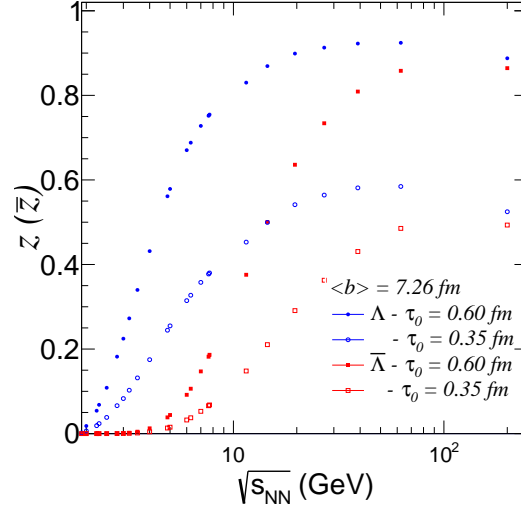
Figure 3. Intrinsic polarization z and $\bar{z}$ for different values of τ_0. The figure is taken from Ref. [19]).

4. Polarization in the Corona $\mathcal{P}^{\Lambda}_{\text{REC}}$ ($\mathcal{P}^{\overline{\Lambda}}_{\text{REC}}$)

As a first approach, we set $\mathcal{P}^{\Lambda}_{\text{REC}} = \mathcal{P}^{\overline{\Lambda}}_{\text{REC}} = 0$, given that, in cold nuclear matter, reactions are less efficient at aligning the spin in the direction of the angular momentum than in the QGP. We can describe the main characteristics of the excitation functions in terms of the ratios $N_{\Lambda\,\text{QGP}}/N_{\Lambda\,\text{REC}}$ ($N_{\overline{\Lambda}\,\text{QGP}}/N_{\overline{\Lambda}\,\text{REC}}$) and $1/(1 + N_{\Lambda\,\text{QGP}}/N_{\Lambda\,\text{REC}})$ ($1/(1 + N_{\overline{\Lambda}\,\text{QGP}}/N_{\overline{\Lambda}\,\text{REC}})$). In central collisions, particle production is dominated by the core region, but as the collision becomes more peripheral, this behaviour reverses. For mid-central collisions, we find that the ratio $N_{\Lambda\,\text{QGP}}/N_{\Lambda\,\text{REC}}$ is smaller than one. It decreases monotonically with the collision energy. On the other hand, the ratio $1/(1 + N_{\Lambda\,\text{QGP}}/N_{\Lambda\,\text{REC}})$ monotonically increases with the collision energy. We notice that the excitation functions peak near where these ratios cross, as shown in Figure 4; the green line, corresponding to $\mathcal{P}^{\Lambda}$, peaks at $\sqrt{s_{NN}} \approx 3$ GeV, where the ratios $N_{\Lambda\,\text{QGP}}/N_{\Lambda\,\text{REC}}$ (purple line) and $1/(1 + N_{\Lambda\,\text{QGP}}/N_{\Lambda\,\text{REC}})$ (blue line) cross. In a similar manner $\mathcal{P}^{\overline{\Lambda}}$, in orange, peaks at $\sqrt{s_{NN}} \approx 6 - 8$ GeV, where the ratios $N_{\overline{\Lambda}\,\text{QGP}}/N_{\overline{\Lambda}\,\text{REC}}$ and $1/(1 + N_{\overline{\Lambda}\,\text{QGP}}/N_{\overline{\Lambda}\,\text{REC}})$ (not shown in the figure) cross. In the case of $\overline{\Lambda}$, this function peaks at a higher collision energy, resulting in a larger polarization than that for the Λs for $\sqrt{s_{NN}} \gtrsim 4$ GeV. This is consistent with experimental data reported by STAR [14]. We could have expected that the $\overline{\Lambda}$ polarization is smaller than the Λ polarization since $\bar{z} < z$, as shown in Figure 3. However, this is not the case, as we show in Ref. [18]; the interplay between the factor $w'/w > 1$ (or $w/w' < 1$) and the ratio $N_{\Lambda\,\text{QGP}}/N_{\Lambda\,\text{REC}} < 1$ amplifies the polarization, producing that $\mathcal{P}^{\Lambda} < \mathcal{P}^{\overline{\Lambda}}$. As is shown in the left panel of Figure 5, the ratio $\mathcal{P}^{\overline{\Lambda}}/\mathcal{P}^{\Lambda}$ increases as w/w' decreases. In the uttermost case in which $z = \bar{z}$ and $N_{\Lambda\,\text{REC}} = N_{\Lambda\,\text{QGP}}$, $\mathcal{P}^{\overline{\Lambda}}$ is always larger than $\mathcal{P}^{\Lambda}$ for $w/w' < 1$. However, for values close to those in mid-central an peripheral collisions, for which $N_{\Lambda\,\text{QGP}}$ becomes smaller than $N_{\Lambda\,\text{REC}}$ and $\bar{z}$ is smaller than z (Figure 3), the ratio $\mathcal{P}^{\overline{\Lambda}}/\mathcal{P}^{\Lambda}$ is still larger than 1 for small enough values of the ratio $w/w' \lesssim 0.1$, which are reached for $\sqrt{s_{NN}} < 10$ GeV. This is shown in the right panel of Figure 5. The explicit expressions for w and w' are shown in Appendices A and B, respectively.
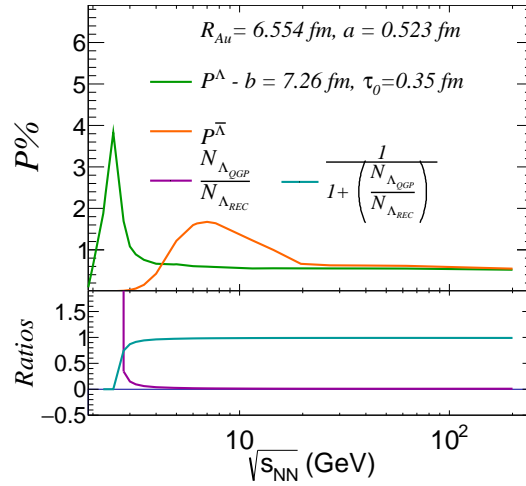
Figure 4. Global polarization $\mathcal{P}^{\Lambda}$ and $\mathcal{P}^{\overline{\Lambda}}$ as functions of collision energy and fixed values of the model parameters.
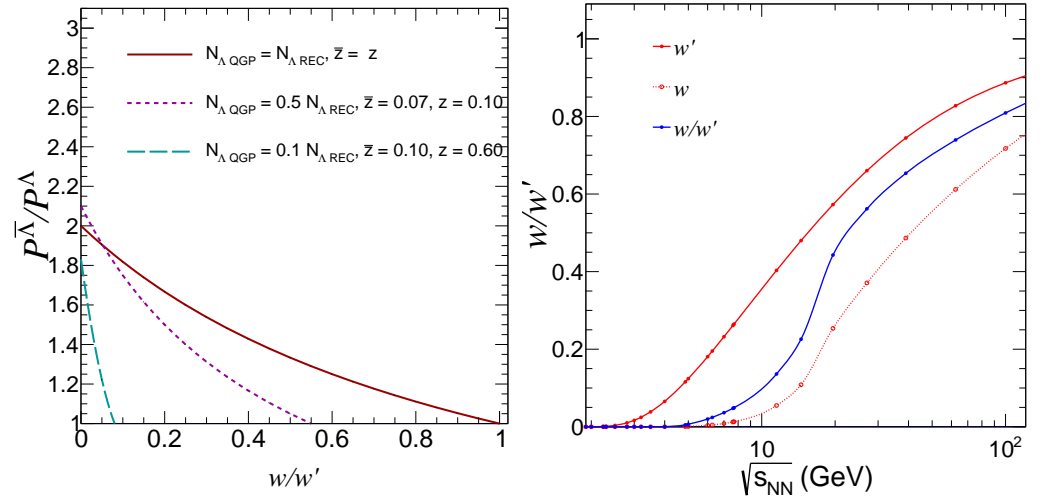
Figure 5. The panel on the left shows that the ratio $\mathcal{P}^{\overline{\Lambda}}/\mathcal{P}^{\Lambda}$ increases as w/w' decreases. For small enough w/w', it achieves values larger than 1 in the case $N_{\Lambda\,\text{QGP}}/N_{\Lambda\,\text{REC}} < 1$, even though $\bar{z} < z$. The panel on the right shows the ratio w/w' as a function of the collision energy.

5. Results

We can now use Equation (5) and the results in the appendices to calculate the global Λ and $\overline{\Lambda}$ polarizations as functions of the collision energy. This is shown in Figure 6.

To compare with the STAR-BES data [14–16], we compute the number of Λs and $\overline{\Lambda}$s, using the expressions in Appendix C, considering the impact parameter interval $b \in (6.66, 10.52)$ fm, which corresponds to the centrality range 20–50%, the scaling constant between the number of $N_{\Lambda\,\text{QGP}}$ created and the $N_{\text{p}\,\text{QGP}}$ number of participants in the collision, $c = 0.0025$, and the radius and skin depth of a gold ion, $R_{Au} = 6.554$ fm and $a = 0.523$ fm, respectively.

The shaded areas in Figure 6 correspond to the regions delimited by fits to the QGP lifetime and volume from Equation (10), used to evaluate the intrinsic polarizations z and $\bar{z}$ considering the thermal vorticity (in Equation (8)) at the corresponding average impact parameter $\langle b \rangle = 8.73$ fm.

Notice that the model calculation gives a good description of experimental data. The difference between the model and HADES data are due to the different centrality intervals. Recall that the magnitude of the polarization decreases for more central collisions, as a consequence of a smaller system vorticity. The maximum of the Λ polarization is close

to its production threshold energy in the $pp \rightarrow \Lambda + K^- + p$ channel, while the $\overline{\Lambda}$ maximum spreads over an interval that in the model depends on the w'/w ratio.
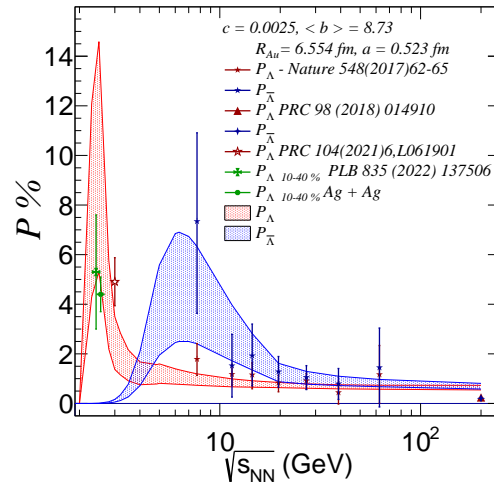
Figure 6. The red and blue shaded regions represent the global polarization $\mathcal{P}^\Lambda$ and $\mathcal{P}^{\overline{\Lambda}}$ as a function of the collision energy for the centrality range 20–50% obtained from the core-corona model. Data from STAR-BES Au+Au [14–16] and HADES Au+Au and Ag+Ag measurements [17].

6. Discussion

We have shown that the core-corona model is successful in describing the general features of the average global polarization measurements for both Λ and $\overline{\Lambda}$. However, the model has limitations for the description of Λ polarization of smaller colliding systems such as Ag + Ag at $\sqrt{s_{NN}} = 2.55$ GeV in the 10–40% centrality class, or for large systems such as Au + Au at small collision energies such as $\sqrt{s_{NN}} = 3$ GeV for centralities larger than 40%. For these conditions, Λs and $\overline{\Lambda}$s in the core are barely produced (see Appendix C), resulting in polarizations that tend to zero. Now, to improve our study, we remove the assumption that the polarization of Λs produced in the corona is negligible, and so now $\mathcal{P}^\Lambda_{REC} \neq 0$ (in the case of $\overline{\Lambda}$, there is no available data at those energies). In fact, from existing data, we know that the contribution can be significant for mid-central or peripheral collisions where $N_{\Lambda\,QGP}/N_{\Lambda\,REC} \rightarrow 0$, and particle production is mainly by pp interactions. In this type of reaction, the transverse polarization does not vanish and the mean polarization in the energy range $\sqrt{s_{NN}} = 10$–63 GeV reaches values of $\mathcal{P} = -0.38 \pm 0.06$ [20].

In Figure 7, we compute $\mathcal{P}^\Lambda$ at $\sqrt{s_{NN}} = 3$ GeV as a function of centrality, where the shaded areas correspond to the values of the intrinsic polarization z computed with Equation (5). We test the sensitivity of the model to a non-negligible $\mathcal{P}^\Lambda_{REC}$ and plot the Λ global polarization with and without a constant contribution of $\mathcal{P}^\Lambda_{REC} = 4\%$. We can already see that there is an improvement in the contributions from the highest centrality intervals when comparing to data for Au + Au at $\sqrt{s_{NN}} = 3$ GeV [16].

If we want to go beyond this test and include a more realistic contribution, we should keep in mind that $\mathcal{P}^\Lambda_{REC}$ is not constant, but, instead, it is a function of centrality and of the collision energy. One way to improve our model in this direction is to take into account the projection of the well-known transverse polarization of Λs produced in the corona (assuming that is similar to the polarization produced in pp collisions) along the direction of the total angular momentum. As we reported in Ref. [21], we found that a non-vanishing average transverse polarization could be linked with a non-vanishing even component of the directed flow. At NICA energies, we have tested this using the MPDroot framework [26,27] and, in a partial analysis, we found non-negligible contributions. This is a work in progress, and a full analysis will be reported elsewhere.
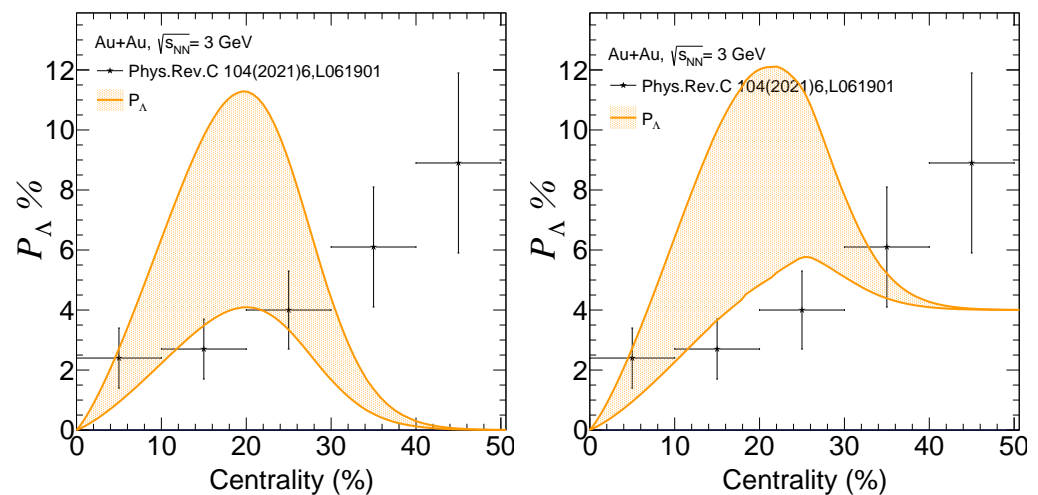
Figure 7. Λ global polarization as a function of centrality. With (right plot) and without (left plot) $\mathcal{P}_{\text{REC}}^{\Lambda} = 4\%$ contribution for all centrality bins. Data for Au+Au at $\sqrt{s_{NN}} = 3$ GeV [16].

7. Conclusions

We have developed a two-component source model dubbed a core-corona model, to explain the excitation function of Λ and $\overline{\Lambda}$ global polarizations. The essential ingredient of this model is the behaviour of the relative abundances $N_{\Lambda\,\text{QGP}}/N_{\Lambda\,\text{REC}}$ in the core and the corona as a function of the collision energy. The intrinsic Λ and $\overline{\Lambda}$ polarizations z and $\bar{z}$, respectively, are computed by means of the relaxation time evaluated from a field theoretical calculation of the quark self-energy in a thermal QCD medium with an effective coupling between the thermal vorticity and the s-quark spin. We obtain different average global polarization for Λs and $\overline{\Lambda}$s, a feature that is not usually found with other approaches. The model also predicts maxima for the polarization excitation functions at HADES and CBM at FAIR and NICA energies. The improvement of the model is a work in progress, and this includes quantifying the contribution from the polarization of the Λs and $\overline{\Lambda}$s coming from the corona region as well as varying the parameters of the model in a consistent manner.

Author Contributions: All the authors contributed equally to this work. All authors have read and agreed to the published version of the manuscript.

Funding: This research was funded by Consejo Nacional de Ciencia y Tecnología Grant No. A1-S-7655 and by UNAM-PAPIIT Grant No. IG100322.

Institutional Review Board Statement: Not applicable.

Informed Consent Statement: Not applicable.

Data Availability Statement: Not applicable.

Acknowledgments: The simulations were produced within the ICN-UNAM cluster and on the basis of the HybriLIT heterogeneous computing platform (LIT, JINR) http://hlit.jinr.ru (accessed on 28 February 2023), (n.d.).

Conflicts of Interest: The authors declare no conflict of interest.

Appendix A. The Ratio w

We model the production of Λ and $\overline{\Lambda}$ in the corona like to happen in the same manner as in that of pp collisions. The ratio w is obtained from the fit to pp experimental data as a function of the center of mass energy, and is given by

$$w = \begin{cases} 0 & \text{for} \quad \sqrt{s} < \sqrt{s_{th}}, \\ \alpha(\sqrt{s} - \sqrt{s_{th}})^2 & \text{for} \quad \sqrt{s_{th}} < \sqrt{s} < 15\,\text{GeV}, \\ A\tanh(\sqrt{s} - \sqrt{s_{th}}) + B\ln(\sqrt{s} - \sqrt{s_{th}}) + C\ln(\sqrt{s} - \sqrt{s_{th}})^2 & \text{for} \quad 15\,\text{GeV} < \sqrt{s} \end{cases} \tag{A1}$$

where $\alpha = 0.0010 \pm 0.0003$, $A = -0.8603 \pm 0.0965$, $B = 0.4935 \pm 0.0314$, $C = -0.0324 \pm 0.0024$ and $\sqrt{s_{th}}$ is the threshold energy to produce a $\overline{\Lambda}$ in the reaction $pp \to pp + \Lambda + \overline{\Lambda}$ [19].

Appendix B. The Ratio w'

We model w' as the ratio of the equilibrium distributions of quarks $\bar{s}$ to s given in terms of its mass $m_s = 100$ MeV, the temperature T and chemical potential as one third of the baryon chemical potential $\mu = \mu_B/3$. This can be written as

$$w' = \frac{e^{(m_s - \mu)/T} + 1}{e^{(m_s + \mu)/T} + 1}. \tag{A2}$$

We compute the w' ratio at the freeze-out temperature and baryon chemical potential parametrized by [28,29]

$$\begin{aligned} T(\mu_B) &= 0.166 - 0.139\mu_B^2 - 0.053\mu_B^4, \\ \mu_B(\sqrt{s_{NN}}) &= \frac{1.308}{1 + 0.273\sqrt{s_{NN}}} \end{aligned} \tag{A3}$$

where T, μ_B and $\sqrt{s_{NN}}$ are expressed in GeV.

Appendix C. Λ and $\overline{\Lambda}$ Production in the Core and Corona

We calculate the relative abundance of Λs produced in the core with respect to the corona $N_{\Lambda\,\text{QGP}}/N_{\Lambda\,\text{REC}}$ with a Glauber model. This allows us to determine the density of participant nucleons in the collision $n_p(\vec{s}, \vec{b})$ at some position $\vec{s}$ in the transverse plane of the collision, as a function of the impact parameter $\vec{b}$. The density n_p is expressed in terms of the thickness functions T_A and T_B of the colliding system $A + B$ as

$$n_p(\vec{s}, \vec{b}) = T_A(\vec{s})[1 - e^{-\sigma_{NN}(\sqrt{s_{NN}})T_B(\vec{s}-\vec{b})}] + T_B(\vec{s} - \vec{b})[1 - e^{-\sigma_{NN}(\sqrt{s_{NN}})T_A(\vec{s})}], \tag{A4}$$

with $T_A(\vec{s}) = \int_\infty^\infty \rho_A(z, \vec{s})dz$ and ρ_A taken as a Woods–Saxon distribution with a skin depth $a = 0.523$ fm and a radius $R = 6.554$ fm for the Au nucleus. σ_{NN} is the collision energy-dependent N + N cross-section, given by the standard PDG parametrization for $\sqrt{s} > 5$ GeV [30], whereas, for $\sqrt{s} < 5$ GeV, we take it as reported in Refs. [31,32].

We introduce a critical density of participants $n_c = 3.3$ fm^{-2} above (below) which the QGP is (is not) formed. Then, we compute the number of Λs produced in the corona as

$$N_{\Lambda\,\text{REC}} = \sigma_{NN}^\Lambda(\sqrt{s}) \int d^2 s\, T_B(\vec{b} - \vec{s}) T_A(\vec{s}) \times \Theta[n_c - n_p(\vec{s}, \vec{b})] \tag{A5}$$

corresponding to the product of the N + N $\to \Lambda$ inclusive cross section σ_{NN}^Λ times the number of N + N collisions, in the region where $n_p < n_c$. For the σ_{NN}^Λ, we take a fit of experimental data in pp collisions given by $\sigma_{pp}^\Lambda = (A\ln\sqrt{s}^2 + B\ln\sqrt{s} + C)\tanh D(0.7\sqrt{s})^E$ with $A = -0.2655 \pm 0.0355$, $B = 2.812 \pm 0.1543$, $C = -2.48 \pm 0.1255$, $D = 0.1058 \pm 0.387$ and $E = 2.01 \pm 0.3308$ [19].

For Λs created in the core, recall that the average number of strange quarks produced in the QGP scales with the number of participants $N_{p\,\text{QGP}}$ in the collision roughly as $\langle s \rangle = N_{\Lambda\,\text{QGP}} = cN_{p\,\text{QGP}}$, where c is in the range $0.001 \le c \le 0.005$ [33]. For this work, we use

$c = 0.0025$ to account for the fact that Λs are not the only strange hadrons produced in the reaction. The number of participants in the QGP is given by

$$N_{\mathrm{p\,QGP}} = \int d^2s\, n_p(\vec{s}, \vec{b}) \Theta[n_p(\vec{s}, \vec{b}) - n_c]. \tag{A6}$$

References

1. Jacob, M. Lambda (anti-lambda) longitudinal polarization: A signature for the formation of a quark—Gluon plasma in heavy ion collisions. *Zeitschrift Phys. Part. Fields* **1988**, *38*, 273–276. [CrossRef]
2. Barros, Jr., C.d.C.; Hama, Y. Λ and $\bar{\Lambda}$ polarization in Au-Au collisions at RHIC. *Phys. Lett. B* **2011**, *699*, 74–77. [CrossRef]
3. Ladygin, V.P.; Jerusalimov, A.P.; Ladygina, N.B. Polarization of Lambda0 hyperons in nucleus-nucleus collisions at high energies. *Phys. Part. Nucl. Lett.* **2010**, *7*, 349–354. [CrossRef]
4. Becattini, F.; Csernai, L.; Wang, D.J. Λ polarization in peripheral heavy ion collisions. *Phys. Rev. C* **2013**, *88*, 034905. Erratum in *Phys. Rev. C* **2016**, *93*, 069901. [CrossRef]
5. Xie, Y.; Glastad, R.C.; Csernai, L.P. Λ polarization in an exact rotating and expanding fluid dynamical model for peripheral heavy ion reactions. *Phys. Rev. C* **2015**, *92*, 064901. [CrossRef]
6. Karpenko, I.; Becattini, F. Study of Λ polarization in relativistic nuclear collisions at $\sqrt{s_{\mathrm{NN}}} = 7.7$ –200 GeV. *Eur. Phys. J. C* **2017**, *77*, 213. [CrossRef]
7. Xie, Y.L.; Bleicher, M.; Stöcker, H.; Wang, D.J.; Csernai, L.P. Λ polarization in peripheral collisions at moderate relativistic energies. *Phys. Rev. C* **2016**, *94*, 054907. [CrossRef]
8. Jiang, Y.; Lin, Z.W.; Liao, J. Rotating quark-gluon plasma in relativistic heavy ion collisions. *Phys. Rev. C* **2016**, *94*, 044910. Erratum in *Phys. Rev. C* **2017**, *95*, 049904. [CrossRef]
9. Shi, S.; Li, K.; Liao, J. Searching for the Subatomic Swirls in the CuCu and CuAu Collisions. *Phys. Lett. B* **2019**, *788*, 409–413. [CrossRef]
10. Li, H.; Pang, L.G.; Wang, Q.; Xia, X.L. Global Λ polarization in heavy-ion collisions from a transport model. *Phys. Rev. C* **2017**, *96*, 054908. [CrossRef]
11. Karpenko, I.; Becattini, F. Vorticity in the QGP liquid and Λ polarization at the RHIC Beam Energy Scan. *Nucl. Phys. A* **2017**, *967*, 764–767. [CrossRef]
12. Xia, X.L.; Li, H.; Tang, Z.B.; Wang, Q. Probing vorticity structure in heavy-ion collisions by local Λ polarization. *Phys. Rev. C* **2018**, *98*, 024905. [CrossRef]
13. Suvarieva, D.; Gudima, K.; Zinchenko, A. A Monte Carlo Study of Lambda Hyperon Polarization at BM@N. *Phys. Part. Nucl. Lett.* **2018**, *15*, 182–188. [CrossRef]
14. Adamczyk, L.; Adkins, J.K.; Agakishiev, G.; Aggarwal, M.M.; Ahammed, Z.; Ajitan, ; N.N.; Alekseev, I.; Anderson, D.M.; Aoyama, R.; Aparin, A.; et al. Global Λ hyperon polarization in nuclear collisions: evidence for the most vortical fluid. *Nature* **2017**, *548*, 62–65. [CrossRef]
15. Adam, J.; Adamczyk, L.; Adams, J.R.; Adkins, J.K.; Agakishiev, G.; Aggarwal, M.M.; Ahammed, Z.; Ajitan, ; N.N.; Alekseev, I.; Anderson, D.M.; et al. Global polarization of Λ hyperons in Au+Au collisions at $\sqrt{s_{NN}} = 200$ GeV. *Phys. Rev. C* **2018**, *98*, 014910. [CrossRef]
16. Yassine, R.A.; Adamczewski-Musch, J.; Asal, C.; Becker, M.; Belounnas, A.; Blanco, A.; Blume, C.; Chlad, L.; Chudoba, P.; Ciepał, I.; et al. Global Λ-hyperon polarization in Au+Au collisions at $\sqrt{s_{NN}}$=3 GeV. *Phys. Rev. C* **2021**, *104*, L061901. [CrossRef]
17. Yassine, R.A.; Adamczewski-Musch, J.; Asal, C.; Becker, M.; Belounnas, A.; Blanco, A.; Blume, C.; Chlad, L.; Chudoba, P.; Ciepal, I.; et al. Measurement of global polarization of Λ hyperons in few-GeV heavy-ion collisions. *Phys. Lett. B* **2022**, *835*, 137506. [CrossRef]
18. Ayala, A.; Torres, M.A.A.; Cuautle, E.; Dominguez, I.; Sanchez, M.A.F.; Maldonado, I.; Moreno-Barbosa, E.; Nieto-Marín, P.A.; Rodriguez-Cahuantzi, M.; Salinas, J.; et al. Core meets corona: A two-component source to explain Λ and $\bar{\Lambda}$ global polarization in semi-central heavy-ion collisions. *Phys. Lett. B* **2020**, *810*, 135818. [CrossRef]
19. Ayala, A.; Domínguez, I.; Maldonado, I.; Tejeda-Yeomans, M.E. Rise and fall of Λ and Λ^- global polarization in semi-central heavy-ion collisions at HADES, NICA and RHIC energies from the core-corona model. *Phys. Rev. C* **2022**, *105*, 034907. [CrossRef]
20. Ayala, A.; Domínguez, I.; Maldonado, I.; Tejeda-Yeomans, M.E. Λ and Λ^- global polarization from the core-corona model. *Rev. Mex. Fis. Suppl.* **2022**, *3*, 040914. [CrossRef]
21. Ayala, A.; Domínguez, I.; Maldonado, I.; Tejeda-Yeomans, M.E. Core-corona approach to describe hyperon global polarization in semi-central relativistic heavy-ion collisions. **2023**. arXiv:2301.07356. [CrossRef]
22. Ayala, A.; De La Cruz, D.; Hernández-Ortíz, S.; Hernández, L.A.; Salinas, J. Relaxation time for quark spin and thermal vorticity alignment in heavy-ion collisions. *Phys. Lett. B* **2020**, *801*, 135169. [CrossRef]
23. Ayala, A.; de la Cruz, D.; Hernández, L.A.; Salinas, J. Relaxation time for the alignment between the spin of a finite-mass quark or antiquark and the thermal vorticity in relativistic heavy-ion collisions. *Phys. Rev. D* **2020**, *102*, 056019. [CrossRef]
24. Bass, S.A.; Belkacem, M.; Bleicher, M.; Br, stetter, M.; Bravina, L.; Ernst, C.; Gerl, ; L.; Hofmann, M.; Hofmann, S.; Konopka, J.; et al. Microscopic models for ultrarelativistic heavy ion collisions. *Prog. Part. Nucl. Phys.* **1998**, *41*, 255–369. [CrossRef]

25. Bleicher, M.; Zabrodin, E.; Spieles, C.; Bass, S.A.; Ernst, C.; Soff, S.; Bravina, L.; Belkacem, M.; Weber, H.; Stöcker, H.; et al. Relativistic hadron hadron collisions in the ultrarelativistic quantum molecular dynamics model. *J. Phys. G* **1999**, *25*, 1859–1896. [CrossRef]
26. Rogachevsky, O.V.; Bychkov, A.V.; Krylov, A.V.; Krylov, V.A.; Moshkin, A.A.; Voronyuk, V.V. Software Development and Computing for the MPD Experiment. *Phys. Part. Nucl.* **2021**, *52*, 817–820. [CrossRef]
27. MpdRoot Framework. Available online: https://mpdroot.jinr.ru (accessed on 30 January 2023).
28. Cleymans, J.; Oeschler, H.; Redlich, K.; Wheaton, S. Comparison of chemical freeze-out criteria in heavy-ion collisions. *Phys. Rev. C* **2006**, *73*, 034905. [CrossRef]
29. Randrup, J.; Cleymans, J. Maximum freeze-out baryon density in nuclear collisions. *Phys. Rev. C* **2006**, *74*, 047901. [CrossRef]
30. Hagiwara, K.; Hikasa, K.; Nakamura, K.; Tanabashi, M.; Aguilar-Benitez, M.; Amsler, C.; Barnett, R.; Burchat, P.R.; Carone, C.D.; Caso, C.; et al. Review of particle physics. *J. Phys. G* **2010**, *37*, 075021. [CrossRef]
31. Buss, O.; Gaitanos, T.; Gallmeister, K.; van Hees, H.; Kaskulov, M.; Lalakulich, O.; Larionov, A.B.; Leitner, T.; Weil, J.; Mosel, U. Transport-theoretical Description of Nuclear Reactions. *Phys. Rept.* **2012**, *512*, 1–124. [CrossRef]
32. Bystricky, J.; La France, P.; Lehar, F.; Perrot, F.; Siemiarczuk, T.; Winternitz, P. Energy dependence of nucleon-nucleon inelastic total cross-sections. *J. Phys. Fr.* **1987**, *48*, 1901–1924. [CrossRef]
33. Letessier, J.; Tounsi, A.; Rafelski, J. Impact of QCD and QGP properties on strangeness production. *Phys. Lett. B* **1996**, *389*, 586–594. [CrossRef]